

See discussions, stats, and author profiles for this publication at: <https://www.researchgate.net/publication/275037279>

# Formation and Transmetalation Mechanisms of Homo- and Heterometallic (Fe/Zn) Trinuclear Triple-Stranded Side-by-Side Helicates

ARTICLE in INORGANIC CHEMISTRY · DECEMBER 2014

Impact Factor: 4.76 · DOI: 10.1021/ic502855g

---

CITATION

1

READS

34

## 6 AUTHORS, INCLUDING:



Bidyut Akhuli

Indian Association for the Cultivation of Science

11 PUBLICATIONS 52 CITATIONS

[SEE PROFILE](#)



Barun Jana

Indian Association for the Cultivation of Science

8 PUBLICATIONS 53 CITATIONS

[SEE PROFILE](#)



Subrata Saha

Indian Association for the Cultivation of Science

9 PUBLICATIONS 40 CITATIONS

[SEE PROFILE](#)



Pradyut Ghosh

Indian Association for the Cultivation of Science

108 PUBLICATIONS 2,527 CITATIONS

[SEE PROFILE](#)

# Formation and Transmetalation Mechanisms of Homo- and Heterometallic (Fe/Zn) Trinuclear Triple-Stranded Side-by-Side Helicates

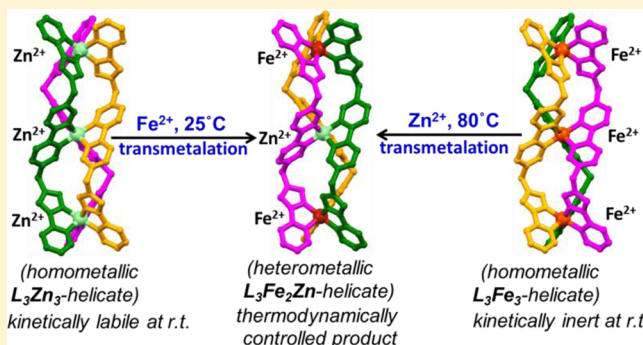
Bidyut Akhuli,<sup>†</sup> Luca Cera,<sup>‡</sup> Barun Jana,<sup>†</sup> Subrata Saha,<sup>†</sup> Christoph A. Schalley,\*<sup>‡</sup> and Pradyut Ghosh\*,<sup>†</sup>

<sup>†</sup>Department of Inorganic Chemistry, Indian Association for the Cultivation of Science, 2A & 2B Raja S. C. Mullick Road, Kolkata 700 032, India

<sup>‡</sup>Institut für Chemie und Biochemie der Freien Universität Berlin, Takustr. 3, 14195 Berlin, Germany

## S Supporting Information

**ABSTRACT:** A novel linear hybrid tris-bidentate neutral ligand having 2,2'-bipyridine and two terminal triazolylpyridine coordination sites (**L**) was efficiently synthesized and explored in the synthesis of trinuclear triple-stranded homometallic side-by-side helicates  $\text{L}_3\text{Fe}_3(\text{OTf})_6$  (**1**) and  $\text{L}_3\text{Zn}_3(\text{OTf})_6$  (**2**), in which the three metal centers display alternating  $\Delta$  and  $\Lambda$  configurations. Selective formation of the analogous heterometallic side-by-side helicate  $\text{L}_3\text{Fe}_2\text{Zn}(\text{OTf})_6$  (**3**) was achieved from a mixture of **L**,  $\text{Fe}(\text{CH}_3\text{CN})_2(\text{OTf})_2$ , and  $\text{Zn}(\text{OTf})_2$  (1:1:1) in acetonitrile at room temperature. Various analytical techniques, i.e., single-crystal X-ray diffraction and NMR and UV-vis spectroscopy, were used to elucidate the sequence of the metal atoms within the heterometallic helicate, with the  $\text{Zn}^{2+}$  at the central position. The formation of **3** was also achieved starting from either  $\text{L}_3\text{Zn}_3(\text{OTf})_6$  or  $\text{L}_3\text{Fe}_3(\text{OTf})_6$  by adding  $\text{Fe}(\text{CH}_3\text{CN})_2(\text{OTf})_2$  or  $\text{Zn}(\text{OTf})_2$ , respectively. ESI-MS and  $^1\text{H}$  NMR studies elucidated different transmetalation mechanisms for the two cases: While a  $\text{Zn}^{2+}$ -to- $\text{Fe}^{2+}$  transmetalation occurs by the stepwise exchange of single ions on the helicate  $\text{L}_3\text{Zn}_3(\text{OTf})_6$  at room temperature, this mechanism is almost inoperative for the  $\text{Fe}^{2+}$ -to- $\text{Zn}^{2+}$  transmetalation in  $\text{L}_3\text{Fe}_3(\text{OTf})_6$ , which is kinetically trapped at room temperature. In contrast, dissociation of  $\text{L}_3\text{Fe}_3(\text{OTf})_6$  at higher temperature is required, followed by reassembly to give  $\text{L}_3\text{Fe}_2\text{Zn}(\text{OTf})_6$ . The reassembly follows an interesting mechanistic pathway when an excess of  $\text{Zn}(\text{OTf})_2$  is present in solution: First,  $\text{L}_3\text{Zn}_3(\text{OTf})_6$  forms as the high-temperature thermodynamic product, which is then slowly converted into the thermodynamic heterometallic  $\text{L}_3\text{Fe}_2\text{Zn}(\text{OTf})_6$  product at room temperature. The temperature-dependent equilibrium shift is traced back to significant entropy differences resulting from an enhancement of the thermal motion of the ligands at high temperature, which destabilize the octahedral iron terminal complex and select zinc in a more stable tetrahedral geometry.



The formation of **3** was also achieved starting from either  $\text{L}_3\text{Zn}_3(\text{OTf})_6$  or  $\text{L}_3\text{Fe}_3(\text{OTf})_6$  by adding  $\text{Fe}(\text{CH}_3\text{CN})_2(\text{OTf})_2$  or  $\text{Zn}(\text{OTf})_2$ , respectively. ESI-MS and  $^1\text{H}$  NMR studies elucidated different transmetalation mechanisms for the two cases: While a  $\text{Zn}^{2+}$ -to- $\text{Fe}^{2+}$  transmetalation occurs by the stepwise exchange of single ions on the helicate  $\text{L}_3\text{Zn}_3(\text{OTf})_6$  at room temperature, this mechanism is almost inoperative for the  $\text{Fe}^{2+}$ -to- $\text{Zn}^{2+}$  transmetalation in  $\text{L}_3\text{Fe}_3(\text{OTf})_6$ , which is kinetically trapped at room temperature. In contrast, dissociation of  $\text{L}_3\text{Fe}_3(\text{OTf})_6$  at higher temperature is required, followed by reassembly to give  $\text{L}_3\text{Fe}_2\text{Zn}(\text{OTf})_6$ . The reassembly follows an interesting mechanistic pathway when an excess of  $\text{Zn}(\text{OTf})_2$  is present in solution: First,  $\text{L}_3\text{Zn}_3(\text{OTf})_6$  forms as the high-temperature thermodynamic product, which is then slowly converted into the thermodynamic heterometallic  $\text{L}_3\text{Fe}_2\text{Zn}(\text{OTf})_6$  product at room temperature. The temperature-dependent equilibrium shift is traced back to significant entropy differences resulting from an enhancement of the thermal motion of the ligands at high temperature, which destabilize the octahedral iron terminal complex and select zinc in a more stable tetrahedral geometry.

## INTRODUCTION

The development of new supramolecular synthetic materials through metal-ion-mediated self-assembly of polydentate ligands is attracting significant interest and has shown great potential for diverse applications in chemistry and materials science.<sup>1–7</sup> Self-assembled helicates are important<sup>8–12</sup> because of their fundamental properties in guest molecule recognition,<sup>13–16</sup> their chirality,<sup>17–22</sup> their magnetic properties,<sup>23–27</sup> and their applications as sensors, DNA binders,<sup>17,28</sup> and anticancer agents.<sup>29</sup> Since the discovery of the first homometallic helicate by Lehn et al. in 1987,<sup>30</sup> different bi- and trinuclear homo- or heterochiral homometallic helicates bearing different transition-metal ions<sup>31–40</sup> as well as f-block elements<sup>13,41–45</sup> have been reported. However, selectively formed heterometallic helicates are still rare in the literature.<sup>35,46–51</sup>

Besides homochiral helicates that have the same chirality at all of the metal centers, there are heterochiral mesocates comprising an even number of metal centers with a mirror plane at the center of the helicate,<sup>52–55</sup> which makes them achiral meso forms. If one extends the mesocates into helicates with an odd number of metal centers, another type of helicate is formed in which the metal centers possess alternating  $\Delta$  and  $\Lambda$  chirality. The odd number of metal centers makes the helicate chiral overall, and the ligands do not wind around the helix but rather bind in a parallel zigzag fashion. These complexes are called side-by-side helicates.<sup>10</sup> In order to synthesize side-by-side helicates rather than regular helicates, rigid chelating ligands or ligands with spacers having an odd number of atoms between the chelating units are used.<sup>56</sup> Until now, only two

Received: December 2, 2014

examples of trinuclear triple-stranded  $Mn^{2+}/Co^{2+}$  helicates with alternating  $\Delta$  and  $\Lambda$  chirality using a rigid ligand have been reported.<sup>24,26</sup> In contrast, the development of trinuclear triple-stranded side-by-side homo- and heterometallic helicates with flexible spacers has not yet been explored.

Mechanistic investigations of the formation and transmetalation pathways of side-by-side helicates have not been performed to date. A detailed understanding of these mechanisms, in particular of the reversible interconversion between homo- and heterometallic helicates, will certainly help designing improved strategies for higher-order helicates with desired properties.

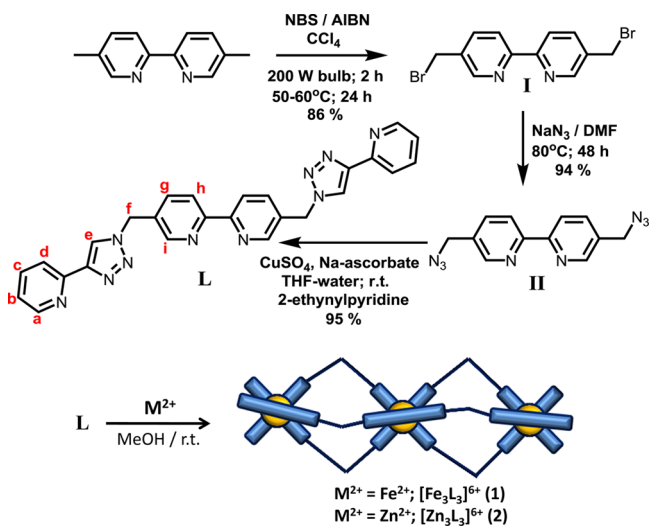
Here we report a hybrid tris-bidentate ligand having one central bipyridyl and two terminal triazolylpyridine chelating units separated by methylene spacers. This ligand forms trinuclear triple-stranded homometallic ( $Fe^{2+}$  or  $Zn^{2+}$ ) and heterometallic ( $Fe^{2+}$  and  $Zn^{2+}$ ) side-by-side helicates. Moreover, detailed mechanistic insight into the transmetalation from the homo- to the heterometallic species is presented.

## RESULTS AND DISCUSSION

**Design Aspects and Ligand Synthesis.** A careful choice of the polytopic ligand and the metal ions is crucial for a spontaneous formation of helicates. Following the “odd–even rule”, one methylene group between two chelating units is expected to favor the formation of a side-by-side helical structure.<sup>56</sup> Furthermore, 2,2'-bipyridine and triazolylpyridines are suitable bidentate chelating ligands for complexation of transition-metal ions. In order to generate heterometallic side-by-side helicates, hybrid ligands combining both binding motifs would be interesting in particular, as one might expect that the preference of each of them for a certain metal ion would lead to a subtle balance that may result in equilibria that can be shifted from homo- to heterometallic helicates. Therefore, the tris-bidentate ligand L under study here (Scheme 1) bears two triazolylpyridine chelating units connected through methylene bridges to a central 5,5'-disubstituted 2,2'-bipyridine.

Another advantage of this design is the facile synthetic access to triazoles by a Huisgen–Sharpless–Meldal click reaction. The tris-bidentate ligand L was synthesized in three steps as depicted in Scheme 1. The reaction of 5,5'-dimethyl-2,2'-

**Scheme 1. Synthesis of Ligand L and the Trinuclear Triple-Stranded Helicates 1 and 2**



bipyridine with *N*-bromosuccinimide (NBS) in  $CCl_4$  in the presence of azobis(isobutyronitrile) (AIBN) gave 5,5'-dibromo-2,2'-bipyridine (I). 5,5'-Diazidomethyl-2,2'-bipyridine (II) was obtained by treating I with sodium azide in *N,N*-dimethylformamide (DMF) at 80 °C. Finally, the click reaction between 2-ethynylpyridine and II in tetrahydrofuran (THF)/ $H_2O$  at room temperature afforded the desired hybrid ligand L. Overall, a yield of 77% was accomplished.

### Trinuclear Triple-Stranded Homometallic Helicates.

To synthesize trinuclear triple-stranded homometallic helicates, solutions of L in dry methanol were treated with 1 equiv of either  $Fe(CH_3CN)_2(OTf)_2$  or  $Zn(OTf)_2$ . With  $Fe^{2+}$ , a deep-red color was observed, consistent with the formation of low-spin  $Fe^{2+}$  complexes that are stable under aerobic conditions. As expected, a colorless complex was formed in case of  $Zn^{2+}$ . The recrystallized products were characterized by elemental analysis; electrospray ionization mass spectrometry (ESI-MS);  $^1H$  correlation spectroscopy (COSY), nuclear Overhauser effect spectroscopy (NOESY), and diffusion-ordered spectroscopy (DOSY) NMR studies; and single-crystal X-ray diffraction.

Figure 1 shows the electrospray ionization Fourier transform ion cyclotron resonance (ESI-FTICR) mass spectra of 1 and 2.

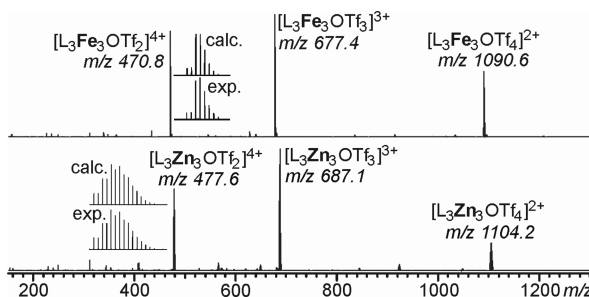


**Figure 1.** FTICR-MS spectra of 20  $\mu M$  methanol solutions of (top) 1 and (bottom) 2. Insets: calculated and experimental isotope patterns.

Characteristic peaks for three different charge states,  $[L_3M_3(OTf)_4]^{2+}$ ,  $[L_3M_3(OTf)_3]^{3+}$ , and  $[L_3M_3(OTf)_2]^{4+}$ , are observed in both cases. The experimental isotope patterns match well with those calculated on the basis of natural abundances.

$^1H$  NMR spectra confirmed the purities of both complexes 1 and 2 (Figure 2). For 1, the  $^1H$  NMR signals of protons a, d, i, and f are shifted upfield and the other signals downfield with respect to those of free ligand L. Similar signal shifts are found for 2, with the notable exception of the signal for proton i. Clearly in both cases 1 and 2, the  $-\text{CH}_2-$  protons are diastereotopic and the corresponding resonance f (a singlet at 5.82 ppm for L) splits into an AB pattern (two doublets centered at 5.58/5.48 ppm and 5.67/5.60 ppm, respectively). In the DOSY NMR spectra of 1 and 2, all of the signals appear at the same diffusion coefficient ( $3.88 \times 10^{-10}$  and  $4.15 \times 10^{-10} \text{ m}^2/\text{s}$ , respectively) and thus belong to a single supramolecular aggregate.

Furthermore, the NOESY spectra of 1 and 2 show two cross-peaks that correspond to i–f and f–g interactions (Figure 3), which are not present in the spectrum of the free ligand and indicate the zigzag arrangement of the ligand along the three metal centers. Each of the two diastereotopic protons f shows a cross-peak to only one of the two protons g and i, in good

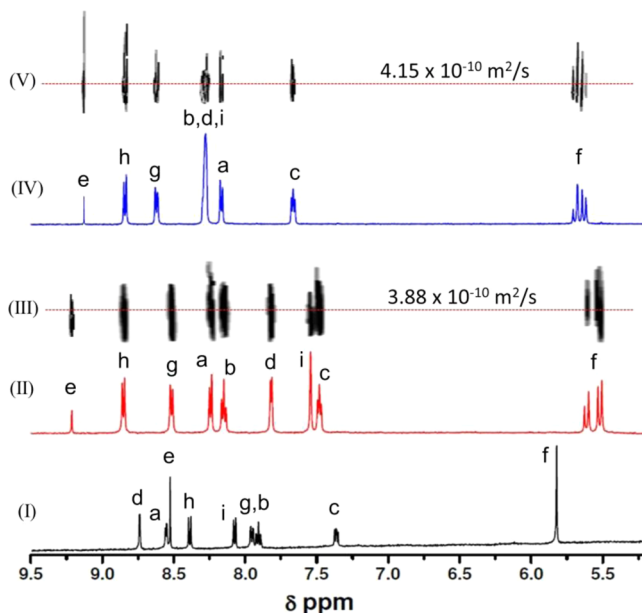


**Figure 2.** (I, II, IV) Partial <sup>1</sup>H NMR spectra of (I) L, (II) 1, and (IV) 2 in MeOH-d<sub>4</sub> at 298 K, showing typical complexation-induced signal shifts. (III, V) DOSY spectra of (III) 1 and (V) 2 with respective diffusion coefficient (*D*) values, indicating the formation of a single supramolecular aggregate in MeOH-d<sub>4</sub> for each helicate.

agreement with the solid-state structure discussed below, in which the N<sub>triazole</sub>—CH<sub>2</sub>—C—CH<sub>i</sub> dihedral angle is 70–95°.

**Single-Crystal X-ray Diffraction.** Single crystals of **1** and **2** suitable for X-ray diffraction studies were obtained when a methanolic solution of the complex was layered over benzene at room temperature. Single-crystal X-ray diffraction analysis of **1** revealed a trinuclear triple-stranded helicate with three Fe<sup>2+</sup> centers arranged in a linear fashion (Figure 4, I). The structure, which is D<sub>3</sub>-symmetric in solution, is slightly distorted in the solid state by packing effects. The side-by-side binding mode of the three nonplanar C<sub>2</sub>-symmetric tris-bidentate ligands around the three octahedral Fe<sup>2+</sup> centers leads to a racemic mixture of heterochiral triple helicates with alternating (Δ, Δ, Δ) and (Δ, Λ, Δ) chirality (Figure 4, II). Helicate **1** crystallizes in the

monoclinic C2/c space group (Table S1 in the Supporting Information). The internuclear Fe1–Fe2 and Fe2–Fe3 distances are found to be 7.67 and 15.33 Å, respectively. The average metal–ligand bond distances for the terminal Fe2 atoms in **1** are Fe2–N<sub>triazole</sub> = 1.92(4) Å and Fe2–N<sub>pyridine</sub> = 1.99(4) Å, while one obtains Fe1–N5 = 1.97(4) Å, Fe1–N10 = 1.96(4) Å, and Fe1–N11 = 1.98(4) Å for the central Fe1 (Table S2 in the Supporting Information).

Single-crystal X-ray diffraction analysis of L<sub>3</sub>Zn<sub>3</sub>(OTf)<sub>6</sub> revealed the formation of a very similar helicate structure (Figure 4, IV). Helicate **2**, however, crystallizes in the triclinic P̄1 space group with intramolecular Zn1–Zn2, Zn1–Zn3, and Zn2–Zn3 distances of 7.77, 7.63, and 15.39 Å, respectively. The average Zn–N bond distances for the terminal Zn2 and Zn3 atoms and the central Zn1 atom in **2** are 2.16 Å (Table S3 in the Supporting Information).

**Photophysical Studies.** The photophysical properties of the two helicates were studied in acetonitrile. The UV-vis spectrum of **1** shows strong bands at  $\lambda_{\text{max}} = 422 \text{ nm}$  ( $\epsilon = 2.36 \times 10^3 \text{ M}^{-1} \text{ cm}^{-1}$ ) and 530 nm ( $\epsilon = 8.13 \times 10^2 \text{ M}^{-1} \text{ cm}^{-1}$ ) (Figure 5, I). The absorption band at 530 nm corresponds to the Fe–bipyridine metal-to-ligand charge transfer (MLCT) transition.<sup>57</sup> Correspondingly, the band at 422 nm is that of the Fe–triazolylpyridine MLCT transition. As expected, the Fe<sup>2+</sup> complexes do not show any emission when excited at 422 and 530 nm. Instead, complex **2** shows a strong emission at 455 nm upon excitation at 300 nm (Figure 5, II). The lifetime of the excited state is about 10 ns. Furthermore, the decay pattern of this complex indicates that only one excited-state species is present (Figure 5, III).

Furthermore, UV-vis titration experiments with Fe<sup>2+</sup> and Zn<sup>2+</sup> ( $\sim 5 \times 10^{-4} \text{ M}$  solution in MeOH) and the tris-bidentate chelating ligand L ( $\sim 5 \times 10^{-5} \text{ M}$  solution in 1:1 CHCl<sub>3</sub>/MeOH) were carried out at room temperature to evaluate the formation constants for the trinuclear triple-stranded homohelicates in solution. The two titration experiments showed a similar spectral feature with a red-shifted absorption band of L in the UV region upon titration with the respective metal ions (Figures S29 and S30 in the Supporting Information). New peaks at 305 and 315 nm appeared during the titrations with Fe<sup>2+</sup> and Zn<sup>2+</sup>, respectively. An isosbestic point at  $\sim 295 \text{ nm}$  in

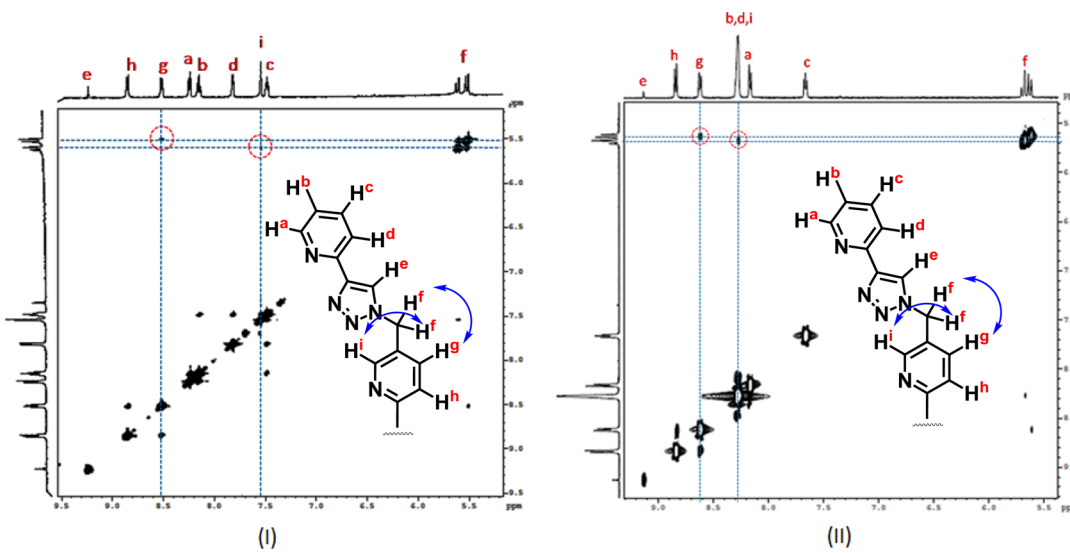


**Figure 3.** 2D NOESY spectra of (I) 1 and (II) 2, in which two through-space <sup>1</sup>H–<sup>1</sup>H couplings are clearly seen.

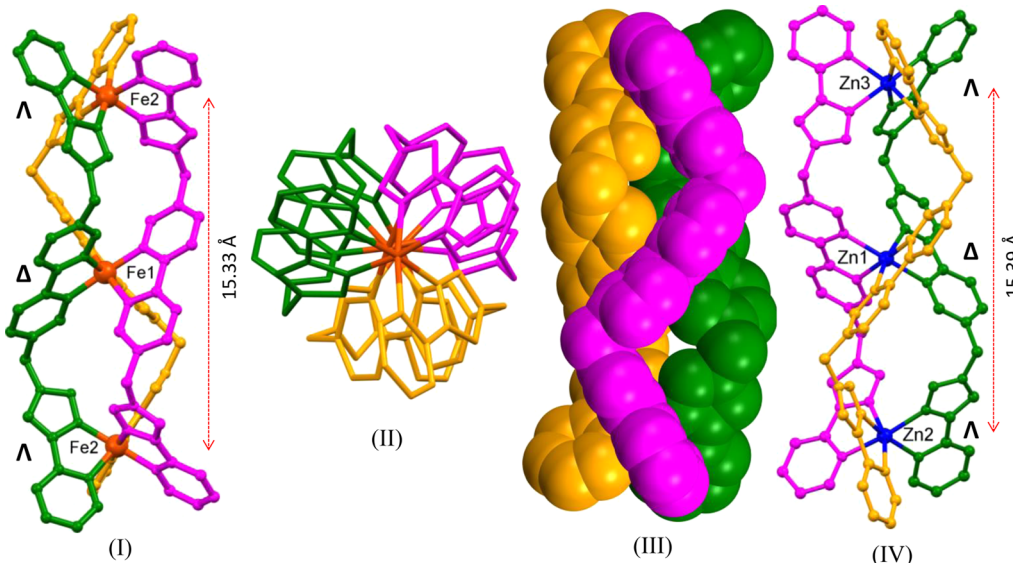


**Figure 4.** Single-crystal X-ray structures of trinuclear triple-stranded helicates **1** (I, front view; II, side view; III, space-filling model) and **2** (IV, front view) showing each ligand strand and the metal coordination octahedra with  $\Lambda$  and  $\Delta$  chirality. Hydrogen atoms, counterions, and solvent molecules are not shown for clarity.

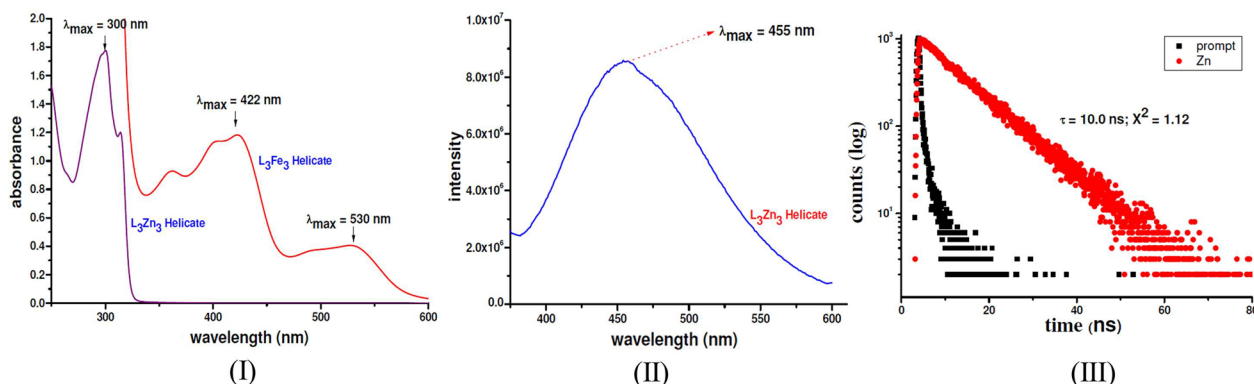


**Figure 5.** (I) UV/vis spectra of complexes **1** ( $5 \times 10^{-4}$  M solution) and **2** ( $5 \times 10^{-5}$  M solution). (II) Emission spectrum of complex **2** ( $10^{-6}$  M solution). (III) Lifetime measurement for complex **2** ( $10^{-6}$  M solution) with respect to a sodium dodecyl sulfate (SDS) prompt in acetonitrile at room temperature.

both cases indicated a single equilibrium that supports the formation of one type of complex in the solution, which could be the formation of the  $M_3L_3$  helicate. The saturation point of the absorbance was achieved upon consumption of  $\sim 1.0$  equiv of the metal ion. Addition of more than 1 equiv of metal ion did not change the absorbance, and thus, no further complexation takes place beyond 1.0 equiv of metal ion. Further, the equivalence plots (plots of absorbance vs equivalents of metal ion; Figures S29 and S30) clearly indicate the formation of 1:1 (i.e.,  $M^{2+}:L = 3:3$ ) complexes in solution, which is consistent with the solid-state single-crystal X-ray structures of the trinuclear triple-stranded helicates of  $Fe^{2+}$  and  $Zn^{2+}$ , in which  $M^{2+}:L = 3:3$ . The UV/vis titration data of **L** with  $Fe^{2+}$  and  $Zn^{2+}$  ions were fitted using the nonlinear regression analysis program SPECFIT,<sup>58</sup> which gave good fits for 3:3 stoichiometry (ligand:metal) in both the cases. The overall formation constants ( $K$ ) for  $M_3L_3$  complexes of  $Fe^{2+}$  and  $Zn^{2+}$  were calculated from the above analyses and were found to be  $10^{26.5 \pm 0.2} M^{-5}$  and  $10^{25.6 \pm 0.6} M^{-5}$ , respectively. Thus, the  $Fe_3L_3$  helicate shows a slightly higher overall formation constant value than the  $Zn_3L_3$  helicate.

**Synthesis and Characterization of the Trinuclear Triple-Stranded Heterometallic Helicate.** In this section, our choice of metal ions is  $Fe^{2+}$  and  $Zn^{2+}$  for the formation of heterometallic helicates. This choice was made because  $Zn^{2+}$  and low-spin  $Fe^{2+}$  complexes and the heterometallic complex formed with these ions can easily be monitored by NMR spectroscopy.

The reaction of **L** with  $Fe(CH_3CN)_2(OTf)_2$  and  $Zn(OTf)_2$  in a 1:1:1 ratio in methanol at room temperature yielded a yellowish-red solution, which has a different color compared to the one of  $L_3Fe_3(OTf)_6$  (dark red) and  $L_3Zn_3(OTf)_6$  (colorless) (Figure S31 in the Supporting Information). FTICR-MS results show characteristic peaks at  $m/z$  1095.1, 680.4, and 473.1, corresponding to  $[L_3Fe_2Zn(OTf)_4]^{2+}$ ,  $[L_3Fe_2Zn(OTf)_3]^{3+}$ , and  $[L_3Fe_2Zn(OTf)_2]^{4+}$ , respectively (Figure 6). The experimental and calculated isotope patterns match well and confirm that complex **3** contains two  $Fe^{2+}$  ions and one  $Zn^{2+}$  ion. Furthermore, energy-dispersive X-ray (EDX) analysis of **3** also shows the presence of both Fe and Zn within the complex (Figure S32 in the Supporting Information).

However, two isomers of  $[L_3Fe_2Zn(OTf)_6]$  are possible with respect to the sequence of metal ions: the two  $Fe^{2+}$  ions at the

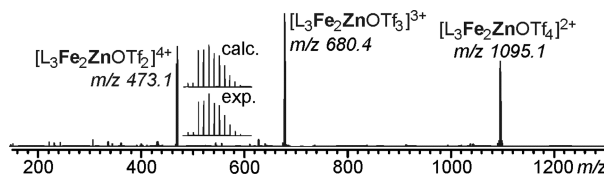


**Figure 6.** FTICR-MS spectrum of a 20  $\mu$ M methanol solution of **3** and (inset) the corresponding isotope pattern of the quadruply charged ion.

terminal triazolylpyridine sites and the  $Zn^{2+}$  ion at the central bipyridine position (Figure 7, I) or the two  $Fe^{2+}$  ions placed next to each other and the  $Zn^{2+}$  ion in one of the terminal triazolylpyridine sites (Figure 7, III). A comparison of the  $^1H$  NMR spectrum of heterometallic helicate **3** with the  $^1H$  NMR spectra of homometallic helicates **1** and **2** (Figure 7, II) clearly supports the symmetric distribution of the metal ions with  $Zn^{2+}$  at the central position. A close match between the  $^1H$  NMR spectra of **3** and **1** is found for the set of proton signals a, b, c, d, and e belonging to the pyridine–triazole aromatic moiety, while very similar chemical shifts in the  $^1H$  NMR spectra of **3** and **2** are observed for protons f and g corresponding to the bipyridine protons.

Furthermore, the solution UV-vis spectrum of  $L_3Fe_2Zn(OTf)_6$  in acetonitrile reveals an absorption band at  $\lambda_{max} = 422$  nm ( $\epsilon = 1.75 \times 10^4 M^{-1} cm^{-1}$ ) (Figure 8, I). The absence of the absorption at 530 nm, which is characteristic of the bipyridine–Fe MLCT transition, demonstrates the presence of  $Zn^{2+}$  at the bipyridine center of the complex. Finally, single-crystal X-ray diffraction of heterometallic helicate **3** confirms the formation of an isostructural trinuclear triple-stranded helicate with two  $Fe^{2+}$  ions located in the two terminal pyridine–triazole centers and  $Zn^{2+}$  at the central bipyridine position (Figure 8, II). The Fe1–Fe2, Fe1–Zn1, and Fe2–Zn1 internuclear distances are 15.46, 7.68, and 7.78 Å, respectively. The average Zn–N bond distance is 2.14 Å, which nicely matches with the corresponding average bond distance of the central  $Zn^{2+}$  ion of the homometallic  $L_3Zn_3(OTf)_6$  helicate (Table S4 in the Supporting Information). The average Fe–N<sub>triazole</sub> and Fe–N<sub>pyridine</sub> bond distances are 1.93 and 2.00 Å, respectively, in line with the corresponding distances in  $L_3Fe_3(OTf)_6$  (Table S4).

**Mechanistic Studies. Formation Pathway of Helicate **3** at Room Temperature.** An equimolar solution of **L**,  $Fe(CH_3CN)_2(OTf)_2$ , and  $Zn(OTf)_2$  in acetonitrile– $d_3$  was monitored over time by  $^1H$  NMR spectroscopy (Figure 9). A comparison of the time-dependent  $^1H$  NMR spectra recorded during the reaction with those of independently prepared samples of helicates **2** and **3** clearly shows the exclusive formation of **3** over the period of a day. Nevertheless, the assembly of other complexes certainly occurs, and over time these complexes converge to **3** and thus must be assembly intermediates. Because of superimposed signals, however, the time-dependent NMR experiments are difficult to interpret in detail. To get more insight into the mechanistic aspects of the formation of the heterometallic helicate, ESI-FTICR mass spectrometry was used to monitor the changes in the solution composition.

First, a 1:2:2 mixture of **L**,  $Zn(OTf)_2$ , and  $Fe(CH_3CN)_2(OTf)_2$  in acetonitrile was monitored over time. After just 15 s of reaction time, the main product is homohelicate **2** ( $m/z$  1104.2, 687.1, and 477.6 for the +2, +3, and +4 charge states). At this stage, only traces of the heterohelicate  $L_3FeZn_2(OTf)_6$  at  $m/z$  683.8 and an intense signal for the 1:1  $LFe(OTf)_2$  complex at  $m/z$  677.8 are observed (Figure 10, I), while  $L_3Fe_2Zn(OTf)_6$  and  $L_3Fe_3(OTf)_6$  are virtually absent. The initially formed homohelicate **2** is then gradually converted into  $L_3FeZn_2(OTf)_6$  ( $m/z$  683.8) (Figure 10, II). After 2 days, the mixture is almost completely converged into the heterohelicate  $L_3Fe_2Zn(OTf)_6$  ( $m/z$  680.4). Not even a trace of the homohelicate  $L_3Fe_3(OTf)_6$  is detected at  $m/z$  677.4 (Figure 10, III). In marked contrast, the iron homohelicate  $L_3Fe_3(OTf)_6$  forms much more slowly when a solution of  $Fe(CH_3CN)_2(OTf)_2$  and **L** is monitored over time in absence of  $Zn(OTf)_2$  in the system. Interestingly, the reaction proceeds through an  $L_3Fe_2(OTf)_4$  intermediate, which forms within less than 1 h and converges into the final  $L_3Fe_3(OTf)_6$  significantly more slowly (Figure S33 in the Supporting Information). From these results, two conclusions can be drawn: (i)  $L_3Fe_2Zn(OTf)_6$  is the thermodynamic product, and (ii) it is generated through a very quickly formed  $L_3Zn_3(OTf)_6$  intermediate that is afterward converted into the final heterometallic helicate  $L_3Fe_2Zn(OTf)_6$  by two consecutive error-correcting transmetalation reactions.

If this holds true, the formation of the heterometallic helicate  $L_3Fe_2Zn(OTf)_6$  would also be expected from a solution of  $L_3Zn_3(OTf)_6$  and  $Fe(CH_3CN)_2(OTf)_2$  at room temperature.

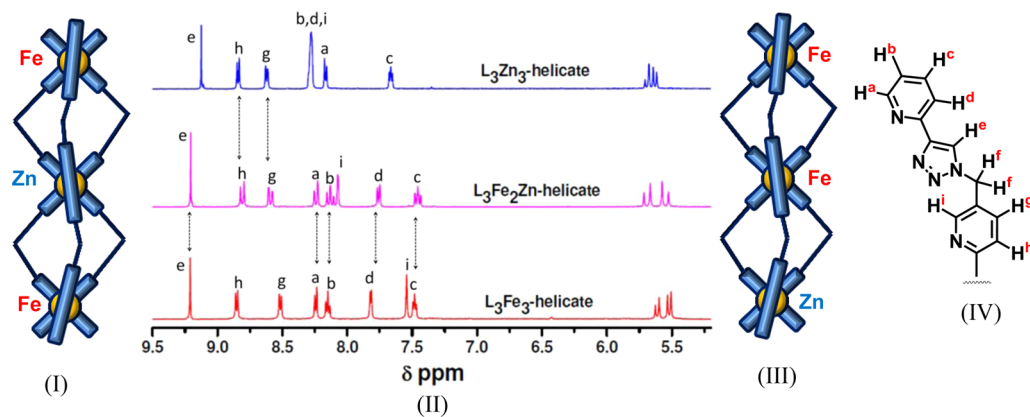


**Figure 7.** (I, III) Graphical representations of the two possible metal ion sequences in  $L_3Fe_2Zn(OTf)_6$ . (II)  $^1H$  NMR spectra of the three complexes in  $MeOH-d_4$  (4.0 mM) at room temperature. (IV) Partial chemical structure of **L** showing the proton assignments.

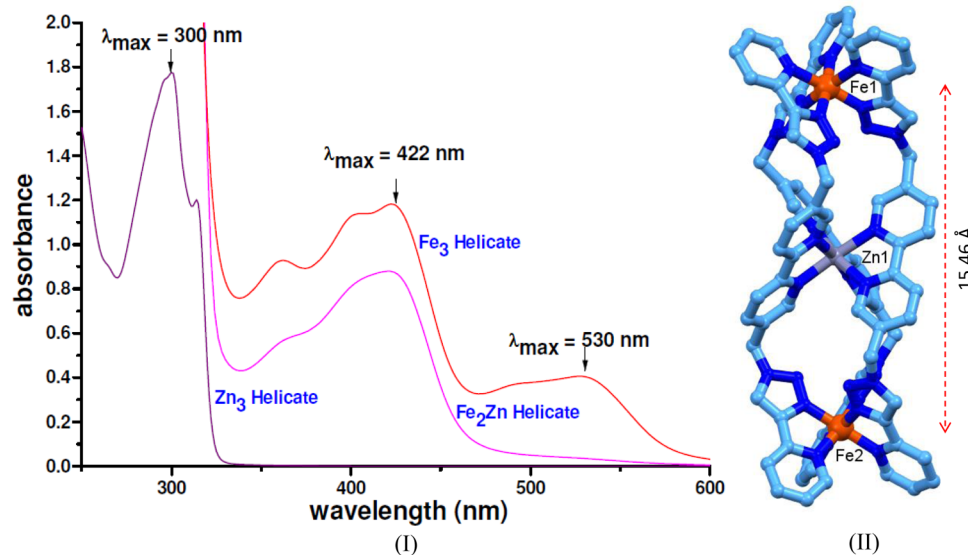


**Figure 8.** (I) UV/vis spectra of the three helicates in acetonitrile at room temperature. The  $\lambda_{\max}$  values are shown. (II) Single-crystal X-ray structure of  $\text{L}_3\text{Fe}_2\text{Zn}(\text{OTf})_6$ .

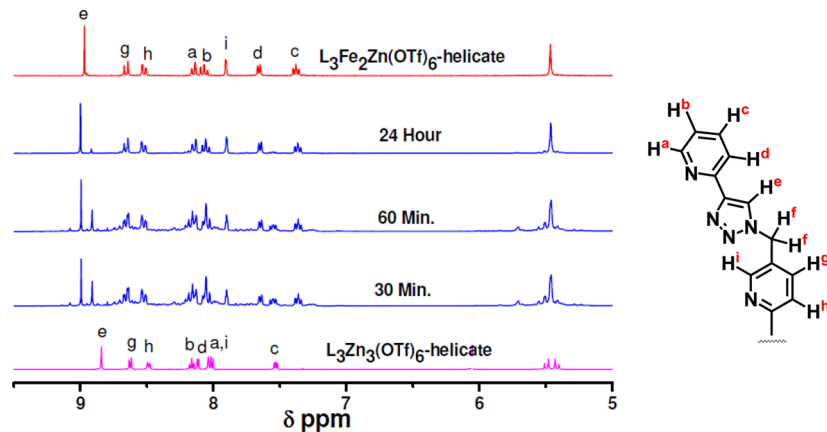


**Figure 9.** Time-dependent <sup>1</sup>H NMR (4.0 mM) spectra recorded for a mixture of L with Zn(OTf)<sub>2</sub> and Fe(CH<sub>3</sub>CN)<sub>2</sub>(OTf)<sub>2</sub> (1:1:1) in acetonitrile-<sup>3</sup>D at room temperature and a comparison with the spectra of  $\text{L}_3\text{Zn}_3(\text{OTf})_6$  and  $\text{L}_3\text{Fe}_2\text{Zn}(\text{OTf})_6$  (4.0 mM).

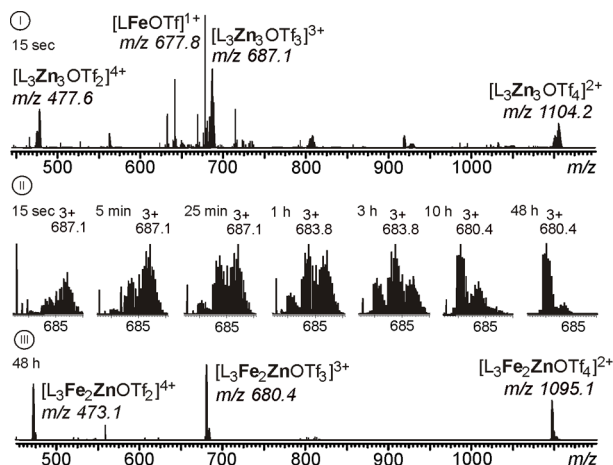


**Figure 10.** (I) ESI-FTICR mass spectrum of a mixture of L, Zn(OTf)<sub>2</sub>, and Fe(CH<sub>3</sub>CN)<sub>2</sub>(OTf)<sub>2</sub> (1:2:2) in acetonitrile solution (20  $\mu$ M in L) after 15 s. (II) Gradual changes in the composition as monitored for the triply charged helicate ions. (III) Final mass spectrum recorded after 48 h.

Indeed, time-dependent <sup>1</sup>H NMR studies carried out on a 1:3 mixture of  $\text{L}_3\text{Zn}_3(\text{OTf})_6$  and Fe(CH<sub>3</sub>CN)<sub>2</sub>(OTf)<sub>2</sub> revealed complete conversion of 2 into 3 after 24 h. Figure 11 shows the time-dependent decrease in the <sup>1</sup>H NMR signal intensities for protons a, b, c, d, e, and i belonging to  $\text{L}_3\text{Zn}_3(\text{OTf})_6$  and the complementary increase in the intensities of a new set of signals closely matching those of the corresponding protons of the heterometallic  $\text{L}_3\text{Fe}_2\text{Zn}(\text{OTf})_6$  helicate. The peak positions of the bipyridine protons g and h do not change during the course of the experiment, confirming that the central Zn<sup>2+</sup> ion does not transmetalate at all during the reaction.

Solution-state UV/vis studies were also carried out to follow the formation of the heterometallic helicate  $\text{L}_3\text{Fe}_2\text{Zn}(\text{OTf})_6$  (Figure 12). Upon addition of Fe(CH<sub>3</sub>CN)<sub>2</sub>(OTf)<sub>2</sub> to the solution of  $\text{L}_3\text{Zn}_3(\text{OTf})_6$  in acetonitrile, time-dependent UV/vis analysis clearly showed the increase in the absorption band at 422 nm ( $\lambda_{\max}$ ) characteristic of the Fe<sup>2+</sup>-triazolylpyridine MLCT transition. Hardly any absorption band around 530 nm characteristic of the Fe<sup>2+</sup>-bipyridine MLCT transition was detected, again ruling out the formation of any  $\text{L}_3\text{Fe}_3(\text{OTf})_6$  helicate in this conversion.

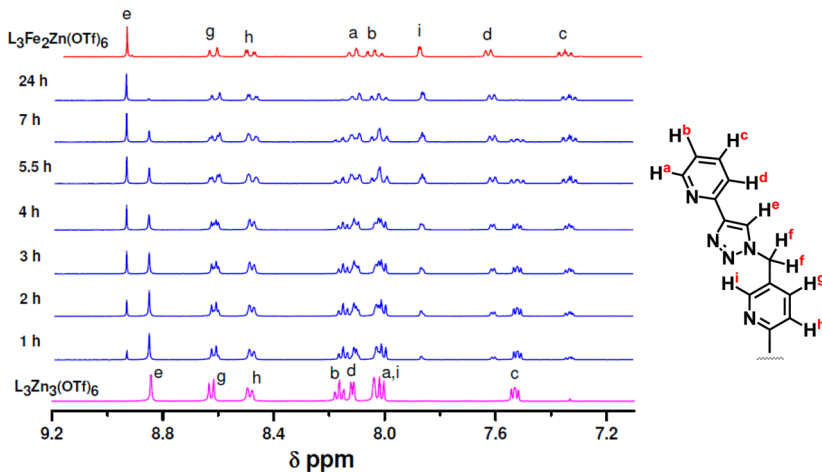


**Figure 11.** Time-dependent  $^1\text{H}$  NMR spectra for the reaction of  $\text{L}_3\text{Zn}_3(\text{OTf})_6$  with  $\text{Fe}(\text{CH}_3\text{CN})_2(\text{OTf})_2$  (1:3) in acetonitrile- $d_3$  at room temperature and a comparison with the spectra of the helicates  $\text{L}_3\text{Zn}_3(\text{OTf})_6$  and  $\text{L}_3\text{Fe}_2\text{Zn}(\text{OTf})_6$  (4.0 mM).

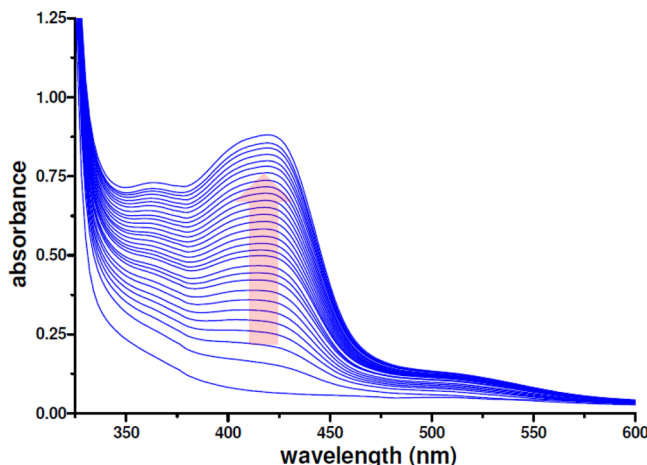


**Figure 12.** Time-dependent UV-vis studies (15 min intervals) of the reaction of  $\text{L}_3\text{Zn}_3(\text{OTf})_6$  with  $\text{Fe}(\text{CH}_3\text{CN})_2(\text{OTf})_2$  (1:3) in acetonitrile at room temperature.

The same reaction was also monitored by ESI-FTICR mass spectrometry. As expected,  $\text{L}_3\text{Zn}_3(\text{OTf})_6$  ( $m/z$  1104.1) was completely consumed over a period of 3 days, leading to the generation of  $\text{L}_3\text{Fe}_2\text{Zn}(\text{OTf})_6$  ( $m/z$  1095.2) via the  $\text{L}_3\text{Zn}_2\text{Fe}(\text{OTf})_6$  intermediate (Figure 13).

In conclusion,  $\text{L}_3\text{Fe}_2\text{Zn}(\text{OTf})_6$  is formed as the thermodynamic product at room temperature, starting from either an equimolar solution of  $\text{Zn}(\text{OTf})_2$ ,  $\text{Fe}(\text{CH}_3\text{CN})_2(\text{OTf})_2$ , and  $\text{L}$  or a solution of  $\text{L}_3\text{Zn}_3(\text{OTf})_6$  and  $\text{Fe}(\text{CH}_3\text{CN})_2(\text{OTf})_2$ . One would therefore also expect the formation of  $\text{L}_3\text{Fe}_2\text{Zn}(\text{OTf})_6$  from a mixture of  $\text{L}_3\text{Fe}_3(\text{OTf})_6$  and  $\text{Zn}(\text{OTf})_2$ . However, when  $\text{L}_3\text{Fe}_3(\text{OTf})_6$  and  $\text{Zn}(\text{OTf})_2$  were mixed in acetonitrile, hardly any transmetalation was observed (Figure 14). Even after a few days at room temperature,  $\text{L}_3\text{Fe}_3(\text{OTf})_6$  was still by far the dominant component. A small percentage of the helicates underwent transmetalation to give  $\text{L}_3\text{Fe}_2\text{Zn}(\text{OTf})_6$ . Even more surprising was the formation of some  $\text{L}_3\text{Zn}_3(\text{OTf})_6$ , while the second intermediate  $\text{L}_3\text{Fe}_2\text{Zn}_2(\text{OTf})_6$  was not observed at all.

While the significantly slower  $\text{Fe}^{2+}$ -to- $\text{Zn}^{2+}$  transmetalation can easily be understood by invoking a higher kinetic stability of the  $\text{Fe}^{2+}$  complex over the  $\text{Zn}^{2+}$  complexes, the surprising distribution of the transmetalation products is more difficult to interpret. Therefore, high-temperature experiments were

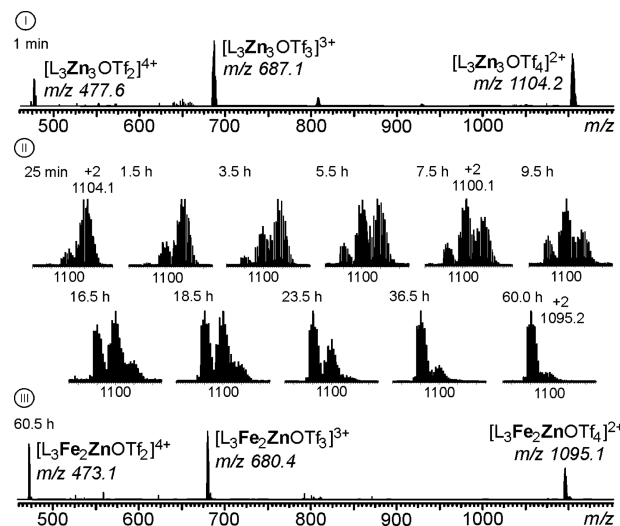


**Figure 13.** (I) ESI-FTICR mass spectrum of a mixture of  $\text{L}_3\text{Zn}_3(\text{OTf})_6$  and  $\text{Fe}(\text{CH}_3\text{CN})_2(\text{OTf})_2$  (1:3) in acetonitrile solution (20  $\mu\text{M}$  in  $\text{L}_3\text{Zn}_3(\text{OTf})_6$ ) after 1 min. (II) Gradual changes in the composition as monitored for the doubly charged helicate ions. (III) Final mass spectrum recorded after 60 h.

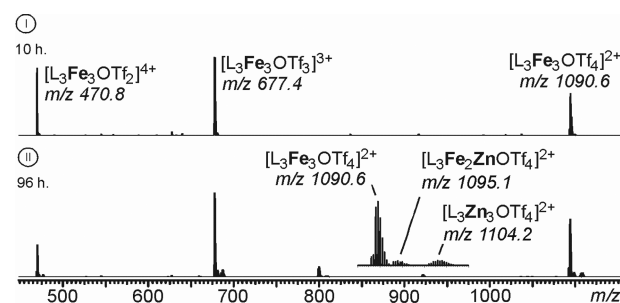


**Figure 14.** ESI-FTICR mass spectra of a mixture of  $\text{L}_3\text{Fe}_3(\text{OTf})_6$  and  $\text{Zn}(\text{OTf})_2$  (1:3) in acetonitrile solution (20  $\mu\text{M}$  in  $\text{L}_3\text{Fe}_3(\text{OTf})_6$ ) at room temperature after (I) 10 h and (II) 96 h.

performed to increase the transmetalation rates and study this reaction in more detail.

**Formation Pathway of Helicate 3 at High Temperature.** For the high-temperature studies, different metal ion stoichiometries were investigated in order to arrive at a more

complete picture of the helicate formation and transmetalation pathways.

When a 1:18 mixture of  $\text{L}_3\text{Fe}_3(\text{OTf})_6$  and  $\text{Zn}(\text{OTf})_2$  in acetonitrile was heated to 80 °C for 1 day and monitored after different time intervals by ESI-FTICR mass spectrometry, the complete transmetalation of all of the  $\text{Fe}^{2+}$  ions to  $\text{Zn}^{2+}$  was observed. After 3 h,  $\text{L}_3\text{Fe}_3(\text{OTf})_6$  was mainly converted into  $\text{L}_3\text{Fe}_2\text{Zn}(\text{OTf})_6$  and  $\text{L}_3\text{FeZn}_2(\text{OTf})_6$ , while only a small amount of  $\text{L}_3\text{Zn}_3(\text{OTf})_6$  was detected. After 6 h,  $\text{L}_3\text{FeZn}_2(\text{OTf})_6$  accumulated and subsequently converted into  $\text{L}_3\text{Zn}_3(\text{OTf})_6$  (Figure 15).

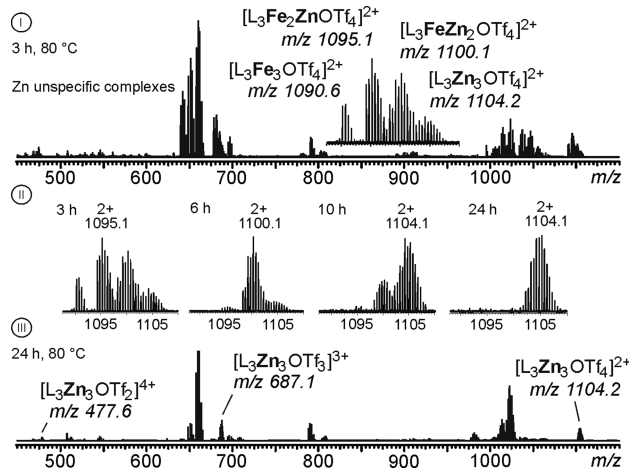


**Figure 15.** (I) ESI-FTICR mass spectrum of a mixture of  $\text{L}_3\text{Fe}_3(\text{OTf})_6$  and  $\text{Zn}(\text{OTf})_2$  (1:18) in acetonitrile solution (20  $\mu\text{M}$  in  $\text{L}_3\text{Fe}_3(\text{OTf})_6$ ) at 80 °C after 3 h. (II) Gradual changes in the composition as monitored for the doubly charged helicate ions. (III) Final mass spectrum recorded after 24 h.

Considering the structure of the helicate and the room-temperature results for the  $\text{Zn}^{2+}$ -free solution discussed above, it is reasonable to assume that the first two exchange steps involve predominantly, if not exclusively, the Fe-triazolylpyridine sites and are followed by a much slower exchange of the central  $\text{Fe}^{2+}$  with  $\text{Zn}^{2+}$ . The same experiment was also monitored by  $^1\text{H}$  NMR spectroscopy, and while the formation of all of the intermediates was hard to follow in detail, the overall replacement of the central  $\text{Fe}^{2+}$  was clearly indicated by the disappearance of the signals of protons c and d (Figure S34 in the Supporting Information).

To further investigate the high-temperature transmetalation,  $\text{L}_3\text{Fe}_3(\text{OTf})_6$  was subjected to the same heating experiment in the presence of a stoichiometric amount of  $\text{Zn}^{2+}$ . When a 1:3 mixture of  $\text{L}_3\text{Fe}_3(\text{OTf})_6$  and  $\text{Zn}(\text{OTf})_2$  in acetonitrile was heated to 80 °C and monitored by ESI-FTICR mass spectrometry, the  $\text{Fe}^{2+}$ -to- $\text{Zn}^{2+}$  transmetalation was again observed, this time finally leading to an equilibrated mixture of all of the possible homo- and heterohelicates within 36 h (Figure 16).

Interestingly,  $\text{L}_3\text{Fe}_3(\text{OTf})_6$ ,  $\text{L}_3\text{Fe}_2\text{Zn}(\text{OTf})_6$ , and  $\text{L}_3\text{Zn}_3(\text{OTf})_6$  were again the only species detected after an intermediate reaction time of 8 h, while  $\text{L}_3\text{FeZn}_2(\text{OTf})_6$  was absent as an intermediate on the way to  $\text{L}_3\text{Zn}_3(\text{OTf})_6$ . This behavior again is surprising in view of the experiment performed with the 1:18 mixture of  $\text{L}_3\text{Fe}_3(\text{OTf})_6$  and  $\text{Zn}(\text{OTf})_2$ , in which the  $\text{L}_3\text{FeZn}_2(\text{OTf})_6$  intermediate slowly converted into the  $\text{L}_3\text{Zn}_3(\text{OTf})_6$  homohelicate at high  $\text{Zn}^{2+}$

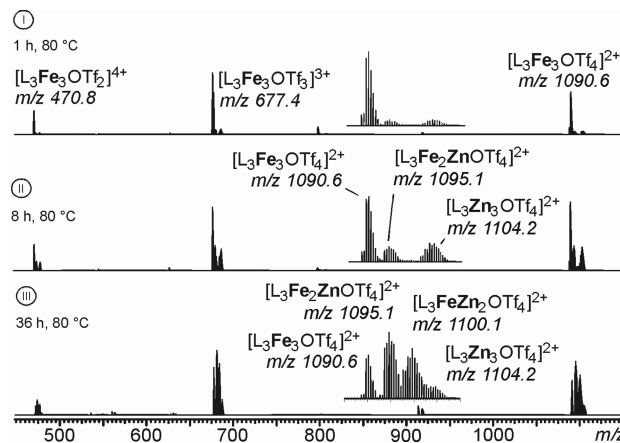


**Figure 16.** ESI-FTICR mass spectra of a mixture of  $\text{L}_3\text{Fe}_3(\text{OTf})_6$  and  $\text{Zn}(\text{OTf})_2$  (1:3) in acetonitrile solution (20  $\mu\text{M}$  in  $\text{L}_3\text{Fe}_3(\text{OTf})_6$ ) at 80 °C after (I) 1 h, (II) 8 h, and (III) 36 h.

concentration. It is unreasonable to assume that this third  $\text{Fe}^{2+}$ -to- $\text{Zn}^{2+}$  exchange becomes faster at lower  $\text{Zn}^{2+}$  concentration. Therefore, the  $\text{L}_3\text{Zn}_3(\text{OTf})_6$  homohelicate observed after 8 h (Figure 16, II) must be formed through a pathway different from a stepwise triple  $\text{Fe}^{2+}$ -to- $\text{Zn}^{2+}$  transmetalation.

Thus, the comparison of the two mixtures monitored at high temperature leads to the conclusion that there are two different pathways for transmetalation (Figure 17). One is certainly a

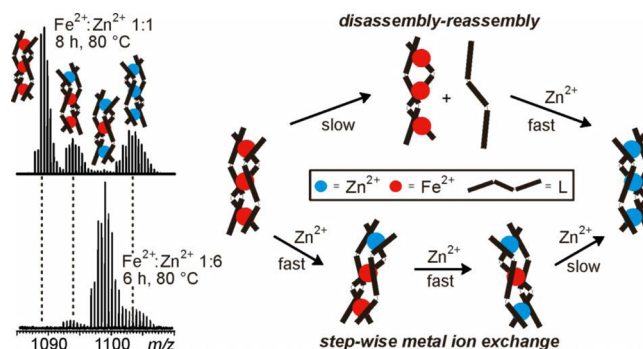


**Figure 17.** (left) Comparison of the ESI-FTICR mass spectra of 1:3 ( $\text{Fe}^{2+}:\text{Zn}^{2+} = 1:1$ ) and 1:18 ( $\text{Fe}^{2+}:\text{Zn}^{2+} = 1:6$ ) mixtures of  $\text{L}_3\text{Fe}_3(\text{OTf})_6$  and  $\text{Zn}(\text{OTf})_2$  at 80 °C acquired after 6 and 8 h, respectively. (right) Representation of the two competing pathways for the formation of  $\text{L}_3\text{Zn}_3(\text{OTf})_6$ .

stepwise metal ion exchange in which initially two terminal  $\text{Fe}^{2+}$  ions are exchanged with  $\text{Zn}^{2+}$  ions, followed by the much slower exchange of the central  $\text{Fe}^{2+}$  ion with  $\text{Zn}^{2+}$ . The second pathway must circumvent this stepwise reaction sequence, and we propose a *disassembly-reassembly* mechanism. Partial dissociation of the helicates leads to the presence of free ligands. As discussed above, the formation of  $\text{L}_3\text{Zn}_3(\text{OTf})_6$  is much faster than the formation of any helicates containing  $\text{Fe}^{2+}$  ions. Thus, the formation of free ligands is quickly followed by the formation of the  $\text{Zn}^{2+}$  homohelicate, which over longer reaction times also back-exchanges to give the  $\text{L}_3\text{FeZn}_2(\text{OTf})_6$  helicate that appears in the final mixture (Figure 16, III).

If this complicated yet intriguing mechanistic scenario holds true, the stoichiometry dependence certainly needs an explanation. If one assumes that the triflate counterions compete with the coordinating ligands to some extent, a

higher concentration of  $\text{Zn}(\text{OTf})_2$  causes stronger competition, in line with the observation that the two terminal  $\text{Fe}^{2+}$  ions are exchanged more quickly in the 1:18 mixture than in the 1:3 mixture. We further propose that the disassembly–reassembly pathway is less strongly affected by the triflate concentration. Therefore, the relative fractions of the helicates that transmetalate through each of the pathways change with the  $\text{Zn}(\text{OTf})_2$  concentration.

Finally, additional evidence for a strong temperature-dependent equilibrium shift comes from an experiment in which the 1:3 mixture of  $\text{L}_3\text{Fe}_3(\text{OTf})_6$  and  $\text{Zn}(\text{OTf})_2$  was first equilibrated at high temperature for 89 h and then stirred at room temperature for additional 40 h. The time-dependent FTICR-MS measurements indeed showed the gradual conversion of  $\text{L}_3\text{Zn}_3(\text{OTf})_6$  and  $\text{L}_3\text{FeZn}_2(\text{OTf})_6$  into  $\text{L}_3\text{Fe}_2\text{Zn}(\text{OTf})_6$  and no further conversion into  $\text{L}_3\text{Fe}_3(\text{OTf})_6$  (Figure 18, II).

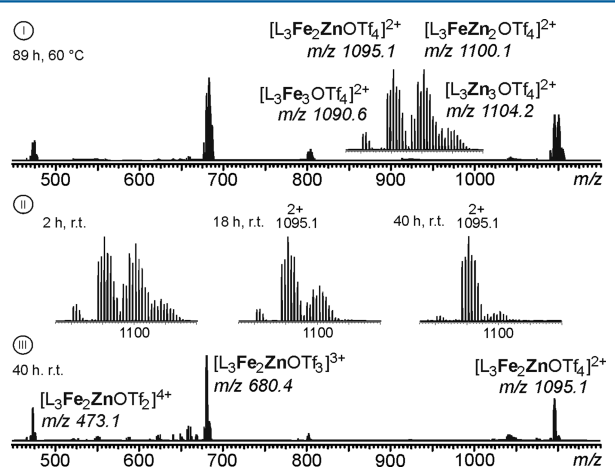


**Figure 18.** (I) ESI-FTICR mass spectrum of a mixture of  $\text{L}_3\text{Fe}_3(\text{OTf})_6$  and  $\text{Zn}(\text{OTf})_2$  (1:3) in acetonitrile solution ( $20 \mu\text{M}$  in  $\text{L}_3\text{Fe}_3(\text{OTf})_6$ ) equilibrated at high temperature. (II) Gradual changes in the composition as monitored for the doubly charged helicate during the  $\text{Zn}^{2+}$ -to- $\text{Fe}^{2+}$  transmetalation at room temperature. (III) Final mass spectrum recorded after 40 h at room temperature.

As expected, the terminal  $\text{Zn}$ –triazolylpyridine complexes undergo a slow  $\text{Zn}^{2+}$ -to- $\text{Fe}^{2+}$  back-transmetalation, while no further replacement of the central  $\text{Zn}^{2+}$  ion is detected. The presence of a  $\text{Zn}^{2+}$  ion at the central position is further indicated by a dramatic decrease in the absorption band at 530 nm corresponding to the  $\text{Fe}$ –bipyridine MLCT transition (Figure 19).

The back-shift of the equilibrium was also observed in the case of a solution of  $\text{L}_3\text{Fe}_3(\text{OTf})_6$  containing excess of  $\text{Zn}(\text{OTf})_2$  (Figure S35 in the Supporting Information). As expected, the  $\text{L}_3\text{Zn}_3(\text{OTf})_6$  homohelicate forms predominantly at high temperature and undergoes back-exchange of the two terminal  $\text{Zn}^{2+}$  at room temperature to become  $\text{L}_3\text{Fe}_2\text{Zn}(\text{OTf})_6$  after 60 h.

The temperature-dependent equilibrium shift can be explained in terms of the different abilities of  $\text{Fe}^{2+}$  and  $\text{Zn}^{2+}$  to form complexes with different coordination numbers. At higher temperature, the increased thermal motion of the ligand preferentially selects the complex with a lower coordination number, which can only be provided by a more stable tetrahedral triazolylpyridine– $\text{Zn}^{2+}$  complex. At room temperature, however, the complex with a higher coordination number

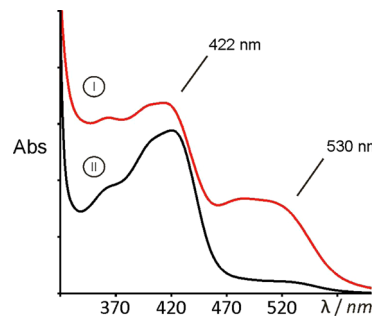


**Figure 19.** UV-vis spectra of (I)  $\text{L}_3\text{Fe}_3(\text{OTf})_6$  in acetonitrile and (II) a mixture of  $\text{L}_3\text{Fe}_3(\text{OTf})_6$  and  $\text{Zn}(\text{OTf})_2$  (1:3) equilibrated at high temperature in acetonitrile after stirring for 40 h at room temperature.

is accessible, which is accomplished by a more stable  $\text{Fe}^{2+}$  complex in an octahedral geometry.

## CONCLUSIONS

We have demonstrated the synthesis of two rare examples of linear trinuclear triple-stranded side-by-side helicates via  $\text{Fe}^{2+}$ / $\text{Zn}^{2+}$ -assisted self-assembly of a newly synthesized linear trisubdinate hybrid ligand having a central 2,2'-bipyridine unit and two terminal triazolylpyridine chelating units. Furthermore, we have reported the first example of heterometallic trinuclear triple-stranded side-by-side helicates. The self-sorting behavior of the hybrid ligand toward the two different metal ions selects the specific formation of  $\text{L}_3\text{Fe}_2\text{Zn}(\text{OTf})_6$ , which can be achieved either at room temperature by mixing of the free components or by conversion of the  $\text{L}_3\text{Fe}_3(\text{OTf})_6$  helicate in the presence of  $\text{Zn}(\text{OTf})_2$  at higher temperature. Indeed, the fast formation of  $\text{L}_3\text{Zn}_3(\text{OTf})_6$  is followed by a slower  $\text{Zn}$ -to- $\text{Fe}$  back-exchange at the terminal positions that leads to the formation of  $\text{L}_3\text{Fe}_2\text{Zn}(\text{OTf})_6$  and no further conversion of the central metal ion. Alternatively,  $\text{L}_3\text{Fe}_2\text{Zn}(\text{OTf})_6$  can be achieved from a solution of  $\text{L}_3\text{Fe}_3(\text{OTf})_6$  by providing the thermal energy necessary to disassemble the helicate scaffold and allowing the replacement of the central  $\text{Fe}^{2+}$  with  $\text{Zn}^{2+}$ . Moreover we have found an unexpectedly pronounced temperature-dependent equilibrium shift between the  $\text{Zn}^{2+}$  and  $\text{Fe}^{2+}$  at the triazolylpyridine metal complex that allows the controlled and reversible formation of  $\text{L}_3\text{Zn}_3(\text{OTf})_6$  at high temperature.

## EXPERIMENTAL SECTION

**Materials and Methods.** ESI-FTICR-MS experiments were done on a Varian/IonSpec QFT-7 instrument. ESI-MS experiments were carried out on a Waters QTOF model YA 263 spectrometer in positive-ion ESI mode. 1D and 2D NMR spectra were recorded on 300/400/500 MHz Bruker DPX NMR spectrometers. All of the reactions were carried out in a dry nitrogen gas atmosphere. The following workup procedures were carried out under ambient conditions. Acetonitrile and methylene chloride were refluxed over  $\text{CaH}_2$  and collected prior to use. DMF was refluxed over  $\text{CaH}_2$ , vacuum-distilled, and stored over molecular sieves.  $\text{Zn}(\text{OTf})_2$  was purchased from Aldrich and used as received.  $\text{Fe}(\text{CH}_3\text{CN})_2(\text{OTf})_2$  was synthesized according to a literature procedure.<sup>59</sup> NBS and AIBN were recrystallized from water and methanol, respectively, prior to use. Deuterated solvents and all other chemicals were used as received from the supplier without further purification.

**X-ray Crystallographic Refinement Details.** Crystals suitable for single-crystal X-ray diffraction studies were selected from the mother liquor, immersed in Paratone oil, mounted on the tip of a glass fiber, and cemented using epoxy resin. Intensity data for the crystals of

**1, 2, and 3** were collected using Mo K $\alpha$  radiation ( $\lambda = 0.7107 \text{ \AA}$ ) on a Bruker SMART APEX II diffractometer equipped with a CCD area detector at 150 K. The data integration and reduction were processed with SAINT software<sup>60</sup> provided with the SMART APEX II software package. An empirical absorption correction was applied to the collected reflections using SADABS.<sup>61</sup> The structures were solved by direct methods using SHELXL<sup>62</sup> and were refined on  $F^2$  by the full-matrix least-squares technique using the SHELXL-97<sup>63</sup> program package. Graphics were generated using PLATON<sup>64</sup> and MERCURY 2.3.<sup>65</sup> Non-hydrogen atoms were refined anisotropically until convergence was reached. In the cases of complexes **1**, **2**, and **3**, the hydrogen atoms were geometrically fixed at idealized positions. For complexes **2** and **3**, we were unable to assign electron density for some solvent molecules in the unit cell, even though the data were collected at 150 K several times. The routine SQUEEZE<sup>66</sup> was applied to the intensity data for both complexes **2** and **3** to take into account the disordered solvent molecules. Again, for complex **2**, one triflate ( $\text{CF}_3\text{SO}_3^-$ ) counteranion (consisting of S8, O13, O14, O15, C84, F10, F11, and F19) was disordered at two sites, and the occupancy factors were refined using the FVAR command of the SHELXTL program and isotropically refined.

**Synthesis of 5,5'-Bis(bromomethyl)-2,2'-bipyridine (I).** This compound was prepared by a modified version of the procedure developed by Tian et al.<sup>67</sup> 5,5'-Dimethyl 2,2'-bipyridine (1 g, 5.43 mmol), NBS (1.932 g, 10.86 mmol), AIBN (445.7 mg, 2.71 mmol), and 200 mL of dry  $\text{CCl}_4$  were mixed in a 250 mL round-bottom flask. The reaction mixture was put on a photoreactor (200 W light bulb) for 1.5 h and then heated to 45–50 °C for 24 h. Subsequently, the reaction mixture was filtered, and the filtrate was dried in vacuo. The crude reaction mixture was separated using silica gel column chromatography in a 25:1  $\text{CH}_2\text{Cl}_2/\text{MeOH}$  mixture. Yield: 1.6 g (86%). ESI-MS(+):  $m/z$  calcd for  $\text{C}_{12}\text{H}_{11}\text{Br}_2\text{N}_2$  [ $\text{M} + \text{H}]^+$  343.04, found 343.08.  $^1\text{H}$  NMR (300 MHz,  $\text{CDCl}_3$ ):  $\delta$  (ppm) 4.55 (s, 4H,  $\text{CH}_2$ ), 8.02 (dd, 2H,  $J = 8.1$  and 2.1 Hz, Ar–CH), 8.63 (d, 2H,  $J = 8.1$  Hz, Ar–CH), 8.78 (d, 2H,  $J = 2.1$  Hz, Ar–CH).  $^{13}\text{C}$  NMR (75 MHz,  $\text{CDCl}_3$ ):  $\delta$  (ppm) 29.56, 121.41, 134.13, 137.89, 149.35, 155.18.

**Synthesis of 5,5'-Bis(azidomethyl)-2,2'-bipyridine (II).** This compound was prepared by a modified version of the procedure developed by Sauvage and co-workers.<sup>68</sup> Dibromide **I** (220 mg, 0.64 mmol) and  $\text{NaN}_3$  (125 mg, 1.93 mmol) were dissolved in 4 mL of dry DMF. The reaction mixture was heated to 80–90 °C for about 2 days and then poured into 150 mL of water. The water phase was extracted with chloroform ( $3 \times 10$  mL). The combined organic phases were dried over anhydrous  $\text{Na}_2\text{SO}_4$ , and the solvent was removed in vacuo to get an off-white solid that was used in the next step without further purification. Yield: 160 mg (94%). ESI-MS(+):  $m/z$  calcd for  $\text{C}_{12}\text{H}_{10}\text{N}_8\text{Na}$  [ $\text{M} + \text{Na}]^+$  289.25, found 289.16.  $^1\text{H}$  NMR (500 MHz,  $\text{CDCl}_3$ ):  $\delta$  (ppm) 4.44 (s, 4H,  $\text{CH}_2$ ), 7.79 (dd, 2H,  $J = 10$  and 3 Hz, Ar–CH), 8.44 (d, 2H,  $J = 10$  Hz, Ar–CH), 8.62 (s, 2H,  $J = 2.1$  Hz, Ar–CH).  $^{13}\text{C}$  NMR (125 MHz,  $\text{CDCl}_3$ ):  $\delta$  (ppm) 52.09, 121.31, 131.50, 136.93, 148.84, 155.66.

**Synthesis of Ligand L.** 200 mg (0.75 mmol) of **II** was dissolved in a mixture of 6 mL of THF and 2 mL of  $\text{H}_2\text{O}$  in a 25 mL round-bottom flask. 2-Ethynylpyridine (160  $\mu\text{L}$ , 1.58 mmol) was added to the solution, followed by sodium ascorbate (310 mg, 1.56 mmol) in 1 mL of  $\text{H}_2\text{O}$  and  $\text{CuSO}_4$  (25 mg, 0.1 mmol) in another 1 mL of  $\text{H}_2\text{O}$ . The reaction mixture was allowed to stir for 12 h under a nitrogen atmosphere. Then 10 mL of a saturated aqueous EDTA solution was added, and the mixture was stirred for another 24 h. The water phase was extracted with dichloromethane ( $3 \times 50$  mL). The combined organic phases were washed two times with brine and dried over  $\text{Na}_2\text{SO}_4$ . The solvent was removed in vacuo to obtain a light-yellow solid that was purified by silica gel (60–120 mesh size) column chromatography using 10% MeOH in  $\text{CH}_2\text{Cl}_2$  with 100  $\mu\text{L}$  of triethylamine in each 100 mL of solvent system. The pure ligand is poorly soluble in all common organic solvents such as dimethyl sulfoxide (DMSO), DMF, MeOH,  $\text{CHCl}_3$ , and  $\text{CH}_3\text{CN}$  but shows moderate solubility in a solvent mixture such as DMSO/ $\text{CHCl}_3$  or MeOH/ $\text{CHCl}_3$ . Yield: 340 mg (95%). ESI-MS(+):  $m/z$  calcd for  $\text{C}_{26}\text{H}_{20}\text{N}_{10}\text{Na}$  [ $\text{M} + \text{Na}]^+$  495.18, found 495.18.  $^1\text{H}$  NMR (DMSO- $d_6$ ,

300 MHz):  $\delta$  (ppm) 5.81 (s, 4H, - $\text{CH}_2^f$ ), 7.32–7.36 (m, 2H, Ar– $\text{CH}^e$ ), 7.86–7.94 (m, 4H, Ar– $\text{CH}^{b,g}$ ), 8.01–8.04 (m, 2H, Ar– $\text{CH}^i$ ), 8.39 (d, 2H,  $J = 8.1$  Hz, Ar– $\text{CH}^h$ ), 8.58–8.60 (m, 2H, Ar– $\text{CH}^d$ ), 8.76–8.78 (m, 4H, Ar– $\text{CH}^{a,e}$ ).  $^1\text{H}$  NMR (MeOH- $d_4$ , 300 MHz):  $\delta$  (ppm) 5.82 (s, 4H,  $\text{CH}_2^f$ ), 7.33–7.38 (m, 2H, Ar– $\text{CH}^e$ ), 7.88–7.97 (m, 4H, Ar– $\text{CH}^{b,g}$ ), 8.06–8.09 (m, 2H, Ar– $\text{CH}^i$ ), 8.39 (d, 2H,  $J = 8.1$  Hz, Ar– $\text{CH}^h$ ), 8.52–8.56 (m, 4H, Ar– $\text{CH}^{a,d}$ ), 8.74 (s, 2H, Ar– $\text{CH}^d$ ).  $^{13}\text{C}$  NMR (DMSO- $d_6$ , 75 MHz):  $\delta$  (ppm) 50.93, 120.03, 121.19, 123.65, 124.17, 137.72, 137.80, 138.02, 148.21, 149.63, 149.77, 150.19, 150.36.

**Synthesis of Helicate 1.** A dry methanol solution of  $\text{Fe}(\text{CH}_3\text{CN})_2(\text{OTf})_2$  (39 mg, 0.089 mmol) was added to a dry methanol (5 mL) suspension of **L** (42 mg, 0.089 mmol) in a round-bottom flask at room temperature. The reaction mixture was allowed to stir in an inert gas atmosphere, and a clear, dark-red solution was obtained after 4 h. The reaction mixture was stirred for an additional 24 h and then filtered through a filter paper. The filtrate was dried, and the red solid was dissolved using 5 mL of methanol. The filtrate was concentrated to 2 mL and layered over benzene (2 mL) in a test tube. Dark-red needle-shaped crystals suitable for single-crystal X-ray measurements were obtained at the interlayer between the two solvents in 12 h. The solvents were removed using a pipet, and the residue was dried under vacuum to get **1** in analytically pure form. Yield: 48 mg (65%). ESI-FTICR-MS:  $m/z$  calcd for  $[\text{Fe}_3\text{L}_3\cdot 4\text{OTf}]^{2+}$  1090.5882, found 1090.5895. Elemental analysis for  $\text{C}_{84}\text{H}_{60}\text{F}_{18}\text{N}_{30}\text{O}_{18}\text{S}_6\text{Fe}_3$ : Found: C, 40.74; H, 2.53; N, 17.03. Calcd: C, 40.69; H, 2.44; N, 16.95.  $^1\text{H}$  NMR (MeOH- $d_4$ , 300 MHz):  $\delta$  (ppm) 5.48 (d, 2H,  $J = 14.5$  Hz,  $\text{CH}_2^f$ ), 5.58 (d, 2H,  $J = 14.0$  Hz,  $\text{CH}_2^f$ ), 7.45 (t, 2H,  $J = 6.5$  Hz, Ar– $\text{CH}^e$ ), 7.51 (s, 2H, Ar– $\text{CH}^i$ ), 7.79 (d, 2H,  $J = 5.5$  Hz, Ar– $\text{CH}^d$ ), 8.12 (t, 2H,  $J = 7.5$  Hz, Ar– $\text{CH}^b$ ), 8.22 (d, 2H,  $J = 8.0$  Hz, Ar– $\text{CH}^a$ ), 8.49 (d, 2H,  $J = 7.0$  Hz, Ar– $\text{CH}^g$ ), 8.82 (d, 2H,  $J = 8.5$  Hz, Ar– $\text{CH}^h$ ), 9.19 (s, 2H, Ar– $\text{CH}^c$ ).  $^{13}\text{C}$  NMR (MeOH- $d_4$ , 75 MHz):  $\delta$  (ppm) 52.95, 121.16, 123.51, 125.91, 127.02, 127.25, 136.58, 140.51, 141.47, 151.45, 154.27, 155.86, 160.72.

**Synthesis of Helicate 2.** A methanol solution of  $\text{Zn}(\text{OTf})_2$  (36.9 mg, 0.10 mmol) was added to a methanol (5 mL) suspension of **L** (48 mg, 0.10 mmol) in a round-bottom flask at room temperature. The reaction mixture was allowed to stir, and a clear, colorless solution was obtained after 30 min. The reaction mixture was stirred for additional 3 h and then filtered through a filter paper. The filtrate was concentrated to 2 mL and layered over benzene (2 mL) in a test tube. Colorless needle-shaped crystals suitable for single-crystal X-ray measurements were obtained at the bottom of the test tube and at the interlayer between the two solvents in 12 h. The solvents were removed using a pipet, and the residue was dried under vacuum to get **2** in analytically pure form. Yield: 67 mg (80%). ESI-FTICR-MS:  $m/z$  calcd for  $[\text{Zn}_3\text{L}_3\cdot 4\text{OTf}]^{2+}$  1104.1393, found 1104.1412. Elemental analysis for  $\text{C}_{84}\text{H}_{60}\text{F}_{18}\text{N}_{30}\text{O}_{18}\text{S}_6\text{Zn}_3$ : Found: C, 40.31; H, 2.49; N, 16.71. Calcd: C, 40.22; H, 2.41; N, 16.75.  $^1\text{H}$  NMR (MeOH- $d_4$ , 500 MHz):  $\delta$  (ppm) 5.59 (d, 2H,  $J = 14$  Hz,  $\text{CH}_2^f$ ), 5.66 (d, 2H,  $J = 14.5$  Hz,  $\text{CH}_2^f$ ), 7.64 (t, 2H,  $J = 6.5$  Hz, Ar– $\text{CH}^e$ ), 8.14 (d, 2H,  $J = 8.5$  Hz, Ar– $\text{CH}^a$ ), 8.24–8.27 (m, 6H, Ar– $\text{CH}^{b,d,i}$ ), 8.59 (d, 2H,  $J = 8.0$  Hz, Ar– $\text{CH}^g$ ), 8.81 (d, 2H,  $J = 8.5$  Hz, Ar– $\text{CH}^h$ ), 9.10 (s, 2H, Ar– $\text{CH}^c$ ).  $^{13}\text{C}$  NMR (MeOH- $d_4$ , 75 MHz):  $\delta$  (ppm) 52.39, 124.12, 125.84, 126.25, 127.68, 136.15, 143.20, 143.90, 144.36, 146.42, 149.50, 150.15, 150.75.

**Synthesis of Helicate 3.** A 5 mL methanol solution of  $\text{Zn}(\text{OTf})_2$  (36.9 mg, 0.10 mmol) and  $\text{Fe}(\text{CH}_3\text{CN})_2(\text{OTf})_2$  (44 mg, 0.10 mmol) was added to a methanol (5 mL) suspension of **L** (48 mg, 0.10 mmol) in a 25 mL round-bottom flask in a dry glovebox at room temperature. A clear straw-yellow solution was obtained after 30 min. The reaction mixture was stirred for additional 24 h and then filtered through a filter paper. The filtrate was dried, and the yellowish-red solid was extracted using 5 mL of methanol. The filtrate was concentrated to 2 mL and layered over benzene (2 mL) in a test tube. Yellowish-red needle-shaped crystals suitable for single-crystal X-ray measurements were obtained at the interlayer between the two solvents in 12 h. The solvents were removed using a pipet, and the residue was dried under vacuum to get **3** in analytically pure form. Yield: 51 mg (62%). ESI-FTICR-MS:  $m/z$  calcd for  $[\text{Fe}_2\text{ZnL}_3\cdot 4\text{OTf}]^{2+}$  1095.0842, found

1095.0860. Elemental analysis for  $C_{84}H_{60}F_{18}Fe_2N_{30}O_{18}S_6Zn$ : Found: C, 40.71; H, 2.49; N, 17.01. Calcd: C, 40.53; H, 2.43; N, 16.88.  $^1H$  NMR ( $MeOH-d_4$ , 300 MHz):  $\delta$  (ppm) 5.47 (s, 4H,  $CH_2'$ ), 7.38 (t, 2H,  $J$  = 6.0 Hz, Ar— $CH'$ ), 7.66 (d, 2H,  $J$  = 6.0 Hz, Ar— $CH^b$ ), 7.90 (d, 2H,  $J$  = 3.0 Hz, Ar— $CH'$ ), 8.07 (t, 2H,  $J$  = 9.0 Hz, Ar— $CH^b$ ), 8.15 (d, 2H,  $J$  = 6.0 Hz, Ar— $CH^a$ ), 8.52 (dd, 2H,  $J$  = 9.0 and 3.0 Hz, Ar— $CH^g$ ), 8.65 (d, 2H,  $J$  = 9.0 Hz, Ar— $CH^h$ ), 8.97 (s, 2H, Ar— $CH^e$ ).  $^{13}C$  NMR ( $MeOH-d_4$ , 75 MHz):  $\delta$  (ppm) 52.57, 123.18, 125.37, 125.89, 126.88, 135.60, 140.15, 143.72, 149.61, 150.19, 150.86, 153.63, 155.77.

## ASSOCIATED CONTENT

### Supporting Information

Crystallographic data (CIF), NMR data, mass data, UV/vis titration experiments, and characterization data. This material is available free of charge via the Internet at <http://pubs.acs.org>.

## AUTHOR INFORMATION

### Corresponding Authors

\*E-mail: c.schalley@fu-berlin.de.

\*E-mail: icpg@iacs.res.in.

### Notes

The authors declare no competing financial interest.

## ACKNOWLEDGMENTS

P.G. gratefully acknowledges the Science and Engineering Research Board (SERB), New Delhi (Project SR/S1/IC-39/2012) for financial support. B.A. acknowledges CSIR for a SRF. Single-crystal X-ray diffraction data were collected at the DBT-funded CEIB Program (Project BT/01/CEIB/11/V/13) awarded to the Department of Organic Chemistry, IACS, Kolkata, India. C.A.S. thanks the Deutsche Forschungsgemeinschaft and Freie Universität Berlin for financial support. We are grateful to the Alexander von Humboldt Foundation for a return fellowship to P.G. We also thank Shahi Imam Reja, Guru Nanak Dev University, India, for his help with the formation constant calculations.

## REFERENCES

- (1) *Metallofoldamers: Supramolecular Architectures from Helicates to Biomimetics*; Maayan, G., Albrecht, M., Eds.; John Wiley & Sons: Chichester, U.K., 2013.
- (2) Carnes, M. E.; Collins, M. S.; Johnson, D. W. *Chem. Soc. Rev.* **2014**, *43*, 1825–1834.
- (3) Beves, J. E.; Campbell, C. J.; Leigh, D. A.; Pritchard, R. G. *Angew. Chem., Int. Ed.* **2013**, *52*, 6464–6467.
- (4) Saalfrank, R. W.; Maid, H.; Scheurer, A. *Angew. Chem., Int. Ed.* **2008**, *47*, 8794–8824.
- (5) Ayme, J.-F.; Beves, J. E.; Leigh, D. A.; McBurney, R. T.; Rissanen, K.; Schultz, D. *J. Am. Chem. Soc.* **2012**, *134*, 9488–9497.
- (6) Ayme, J.-F.; Beves, J. E.; Leigh, D. A.; McBurney, R. T.; Rissanen, K.; Schultz, D. *Nat. Chem.* **2012**, *4*, 15–20.
- (7) Leigh, D. A.; Pritchard, R. G.; Stephens, A. J. *Nat. Chem.* **2014**, *6*, 978–982.
- (8) Boiocchi, M.; Fabbrizzi, L. *Chem. Soc. Rev.* **2014**, *43*, 1835–1847.
- (9) Miyake, H.; Tsukube, H. *Chem. Soc. Rev.* **2012**, *41*, 6977–6991.
- (10) Albrecht, M. *Chem. Rev.* **2001**, *101*, 3457–3497.
- (11) Hannon, M. J.; Childs, L. J. *Supramol. Chem.* **2004**, *16*, 7–22.
- (12) Bunzen, J.; Bruhn, T.; Bringmann, G.; Lützen, A. *J. Am. Chem. Soc.* **2009**, *131*, 3621–3630.
- (13) Wang, B.; Zang, Z.; Wang, H.; Dou, W.; Tang, X.; Liu, W.; Shao, Y.; Ma, J.; Li, Y.; Zhou, J. *Angew. Chem., Int. Ed.* **2013**, *52*, 3756–3759.
- (14) Yamamoto, S.; Iida, H.; Yashima, E. *Angew. Chem., Int. Ed.* **2013**, *52*, 6849–6853.
- (15) Sorensen, A.; Castilla, A. M.; Ronson, T. K.; Pittelkow, M.; Nitschke, J. R. *Angew. Chem., Int. Ed.* **2013**, *52*, 11273–11277.
- (16) Custelcean, R.; Bonnesen, P. V.; Roach, B. D.; Duncan, N. C. *Chem. Commun.* **2012**, *48*, 7438–7440.
- (17) Howson, S. E.; Bolhuis, A.; Brabec, V.; Clarkson, G. J.; Malina, J.; Rodger, A.; Scott, P. *Nat. Chem.* **2012**, *4*, 31–36.
- (18) Kaminker, R.; de Hatten, X.; Lahav, M.; Lupo, F.; Gulino, A.; Evmenenko, G.; Dutta, P.; Browne, C.; Nitschke, J. R.; van der Boom, M. E. *J. Am. Chem. Soc.* **2013**, *135*, 17052–17059.
- (19) Ousaka, N.; Grunder, S.; Castilla, A. M.; Whalley, A. C.; Stoddart, J. F.; Nitschke, J. R. *J. Am. Chem. Soc.* **2012**, *134*, 15528–15537.
- (20) Albrecht, M.; Isaak, E.; Baumert, M.; Gossen, V.; Raabe, G.; Froehlich, R. *Angew. Chem., Int. Ed.* **2011**, *50*, 2850–2853.
- (21) Guetz, C.; Hovorka, R.; Struch, N.; Bunzen, J.; Meyer-Eppler, G.; Qu, Z.-W.; Grimme, S.; Topic, F.; Rissanen, K.; Cetina, M.; Engeser, M.; Lützen, A. *J. Am. Chem. Soc.* **2014**, *136*, 11830–11838.
- (22) Kiehne, U.; Lützen, A. *Org. Lett.* **2007**, *9*, 5333–5336.
- (23) Habib, F.; Long, J.; Lin, P.-H.; Korobkov, I.; Ungur, L.; Wernsdorfer, W.; Chibotaru, L. F.; Murugesu, M. *Chem. Sci.* **2012**, *3*, 2158–2164.
- (24) Dul, M.-C.; Pardo, E.; Lescouezec, R.; Chamoreau, L.-M.; Villain, F.; Journaux, Y.; Ruiz-Garcia, R.; Cano, J.; Julve, M.; Lloret, F.; Pasan, J.; Ruiz-Perez, C. *J. Am. Chem. Soc.* **2009**, *131*, 14614–14615.
- (25) Pardo, E.; Cangussu, D.; Dul, M.-C.; Lescouezec, R.; Herson, P.; Journaux, Y.; Pedroso, E. F.; Pereira, C. L. M.; Munoz, M. C.; Ruiz-Garcia, R.; Cano, J.; Amoros, P.; Julve, M.; Lloret, F. *Angew. Chem., Int. Ed.* **2008**, *47*, 4211–4216.
- (26) Aromi, G.; Berzal, P. C.; Gamez, P.; Roubeau, O.; Kooijman, H.; Spek, A. L.; Driessens, W. L.; Reedijk, J. *Angew. Chem., Int. Ed.* **2001**, *40*, 3444–3446.
- (27) Safin, D. A.; Babashkina, M. G.; Robeyns, K.; Rouzieres, M.; Clerac, R.; Garcia, Y. *Dalton Trans.* **2013**, *42*, 16470–16473.
- (28) Zhao, C.; Wu, L.; Ren, J.; Xu, Y.; Qu, X. *J. Am. Chem. Soc.* **2013**, *135*, 18786–18789.
- (29) Faulkner, A. D.; Kaner, R. A.; Abdallah, Q. M. A.; Clarkson, G.; Fox, D. J.; Gurnani, P.; Howson, S. E.; Phillips, R. M.; Roper, D. I.; Simpson, D. H.; Scott, P. *Nat. Chem.* **2014**, *6*, 797–803.
- (30) Lehn, J. M.; Rigault, A.; Siegel, J.; Harrowfield, J.; Chevrier, B.; Moras, D. *Proc. Natl. Acad. Sci. U.S.A.* **1987**, *84*, 2565–2569.
- (31) Weekes, D. M.; Diebold, C.; Mobian, P.; Huguenard, C.; Allouche, L.; Henry, M. *Chem.—Eur. J.* **2014**, *20*, 5092–5101.
- (32) Roberts, D. A.; Castilla, A. M.; Ronson, T. K.; Nitschke, J. R. *J. Am. Chem. Soc.* **2014**, *136*, 8201–8204.
- (33) Boiocchi, M.; Brega, V.; Ciarrocchi, C.; Fabbrizzi, L.; Pallavicini, P. *Inorg. Chem.* **2013**, *52*, 10643–10652.
- (34) Zhang, Z.; Chen, Y.; Dolphin, D. *Dalton Trans.* **2012**, *41*, 4751–4753.
- (35) Campbell, V. E.; de Hatten, X.; Delsuc, N.; Kauffmann, B.; Huc, I.; Nitschke, J. R. *Nat. Chem.* **2010**, *2*, 684–687.
- (36) Campbell, V. E.; de Hatten, X.; Delsuc, N.; Kauffmann, B.; Huc, I.; Nitschke, J. R. *Chem.—Eur. J.* **2009**, *15*, 6138–6142.
- (37) Hasenkopf, B.; Lehn, J.-M.; Boumediene, N.; Leize, E.; Van Dorsselaer, A. *Angew. Chem., Int. Ed.* **1998**, *37*, 3265–3268.
- (38) Young, M. C.; Johnson, A. M.; Hooley, R. J. *Chem. Commun.* **2014**, *50*, 1378–1380.
- (39) Lützen, A.; Hapke, M.; Griep-Raming, J.; Haase, D.; Saak, W. *Angew. Chem., Int. Ed.* **2002**, *41*, 2086–2089.
- (40) Kiehne, U.; Weilandt, T.; Lützen, A. *Eur. J. Org. Chem.* **2008**, 2056–2064.
- (41) Shu, Y.-B.; Tang, X.-L.; Liu, W.-S. *Inorg. Chem. Front.* **2014**, *1*, 226–230.
- (42) Zeckert, K.; Hamacek, H.; Senegas, J.-M.; Dalla-Favera, N.; Floquet, S.; Bernardinelli, G.; Piguet, C. *Angew. Chem., Int. Ed.* **2005**, *44*, 7954–7958.
- (43) Bocquet, B.; Bernardinelli, G.; Ouali, N.; Floquet, S.; Renaud, F.; Hopfgartner, G.; Piguet, C. *Chem. Commun.* **2002**, 930–931.
- (44) Floquet, S.; Ouali, N.; Bocquet, B.; Bernardinelli, G.; Imbert, D.; Bünzli, J.-C. G.; Hopfgartner, G.; Piguet, C. *Chem.—Eur. J.* **2003**, *9*, 1860–1875.

- (45) Johnson, A. M.; Young, M. C.; Zhang, X.; Julian, R. R.; Hooley, R. J. *J. Am. Chem. Soc.* **2013**, *135*, 17723–17726.
- (46) Hahn, F. E.; Offermann, M.; Isfort, C. S.; Pape, T.; Froehlich, R. *Angew. Chem., Int. Ed.* **2008**, *47*, 6794–6797.
- (47) Cantuel, M.; Gumy, F.; Bünzli, J.-C. G.; Piguet, C. *Dalton Trans.* **2006**, 2647–2660.
- (48) Riis-Johannessen, T.; Bernardinelli, G.; Filinchuk, Y.; Clifford, S.; Dalla Favera, N.; Piguet, C. *Inorg. Chem.* **2009**, *48*, 5512–5525.
- (49) Albrecht, M.; Froehlich, R. *J. Am. Chem. Soc.* **1997**, *119*, 1656–1661.
- (50) Piguet, C.; Hopfgartner, G.; Williams, A. F.; Bünzli, J.-C. G. *J. Chem. Soc., Chem. Commun.* **1995**, 491–493.
- (51) Albrecht, M.; Liu, Y.; Zhu, S. S.; Schalley, C. A.; Froehlich, R. *Chem. Commun.* **2009**, 1195–1197.
- (52) Raja, M.; Iyer, R. G.; Gwengo, C.; Reger, D. L.; Pellechia, P. J.; Smith, M. D.; Pascui, A. E. *Organometallics* **2013**, *32*, 95–103.
- (53) Djeda, R.; Desmarets, C.; Chamoreau, L.-M.; Li, Y.; Journaux, Y.; Gontard, G.; Amouri, H. *Inorg. Chem.* **2013**, *52*, 13042–13047.
- (54) Dul, M.-C.; Lescouezec, R.; Chamoreau, L.-M.; Journaux, Y.; Carrasco, R.; Castellano, M.; Ruiz-Garcia, R.; Cano, J.; Lloret, F.; Julve, M.; Ruiz-Perez, C.; Fabelo, O.; Pardo, E. *CrystEngComm* **2012**, *14*, 5639–5648.
- (55) Cooke, D. J.; Cross, J. M.; Fennessy, R. V.; Harding, L. P.; Rice, C. R.; Slater, C. *Chem. Commun.* **2013**, *49*, 7785–7787.
- (56) Albrecht, M.; Kotila, S. *Angew. Chem., Int. Ed. Engl.* **1995**, *34*, 2134–2137.
- (57) Cagle, F. W., Jr.; Smith, G. F. *J. Am. Chem. Soc.* **1947**, *69*, 1860–1862.
- (58) Gampp, H.; Maeder, M.; Meyer, C. J.; Zhuberbühler, A. D. *Talanta* **1985**, *32*, 95–101.
- (59) Hagen, K. S. *Inorg. Chem.* **2000**, *39*, 5867–5869.
- (60) Sheldrick, G. M. SAINT and XPREP, version 5.1; Siemens Industrial Automation Inc.: Madison, WI, 1995.
- (61) Sheldrick, G. M. SADABS: Empirical Absorption Correction Program; University of Göttingen: Göttingen, Germany, 1997.
- (62) Sheldrick, G. M. SHELLXTL Reference Manual, version 5.1; Bruker AXS: Madison, WI, 1997.
- (63) Sheldrick, G. M. SHELXL-97: Program for Crystal Structure Refinement; University of Göttingen: Göttingen, Germany, 1997.
- (64) Spek, A. L. PLATON-97; University of Utrecht: Utrecht, The Netherlands, 1997.
- (65) Mercury, version 2.3 (supplied with Cambridge Structural Database); CCDC: Cambridge, U.K., 2003–2004.
- (66) Van der Sluis, P.; Spek, A. L. *Acta Crystallogr., Sect. A* **1990**, *46*, 194–201.
- (67) Tian, L.-l.; Wang, C.; Dawn, S.; Smith, M. D.; Krause, J. A.; Shimizu, L. S. *J. Am. Chem. Soc.* **2009**, *131*, 17620–17629.
- (68) Mobian, P.; Collin, J.-P.; Sauvage, J.-P. *Tetrahedron Lett.* **2006**, *47*, 4907–4909.